

# Assessment of Elastic Parameters of Human Skin Using Dynamic Elastography

Jean-Luc Gennisson, Thérèse Baldeweck, Mickaël Tanter, Stefan Catheline, Mathias Fink, Laurent Sandrin, Céline Cornillon, and Bernard Querleux

**Abstract**—Sonoelastography and transient elastography are two ultrasound-based techniques that facilitate noninvasive characterization of the viscoelastic properties of soft tissues by investigating their response to shear mechanical excitation. Young's modulus is the principle assessment parameter. Because it defines local tissue stiffness, it is of major interest for the medical imaging and cosmetic industries as it could replace subjective palpation by yielding local, quantitative information. In this paper, we describe a new high-resolution device capable of measuring local Young's modulus in very thin layers (1–5 mm) and devoted to the *in vivo* evaluation of the elastic properties of human skin. It uses an ultrasonic probe (50 MHz) for tracking the displacements induced by a 300 Hz shear wave generated by a ring surrounding the transducer. The displacements are measured using a conventional cross-correlation technique between successive ultrasonic back-scattered echoes. First, this noninvasive technique has been experimentally proven to be accurate for investigating elasticity in different skin-mimicking phantoms. Second, data were acquired *in vivo* on human forearms. As expected, Young's modulus was found to be higher in the dermis than in the hypodermis and other soft tissues.

## I. INTRODUCTION

THE mechanical properties of the skin play a key role in one main function of the skin: its protective function of the underlying tissues. In dermatology, the severity of many skin diseases (e.g., scleroderma, Ehlers-Danlos, keloids), which induce alterations of the mechanical properties of the skin, can be assessed by measuring, for instance, elastic properties of the connective tissue. In healthy skin, chronological effects and photodamage on the mechanical properties of the skin are becoming all the more important with the increase in life expectancy and the desire to preserve an attractive appearance.

Many *in vitro* techniques have been used in the past to characterize local skin elasticity, but they have not taken into account the natural stretching, tissue moisture, and vascularization of the skin. Several *in vivo* techniques for the noninvasive estimation of Young's skin modulus, therefore, are under development currently, e.g., twisting [1],

friction [2], suction [3], tonometry [4], and wave propagation [5]. The main drawback of these techniques is that their spatially average Young's modulus estimation reveals the mean elastic properties of the entire skin as well as the hypodermis in certain cases. Regarding the approach based on wave propagation, the basic principle consists in applying an electromagnetic device perpendicularly to the skin surface in order to generate a low-frequency elastic surface wave (0–2 kHz). The wave is detected by another electromagnetic device located some millimeters away, and the surface wave speed can be evaluated. Based on this approach, many studies have been put forward to characterize the tissue according to the dependence of wave transmission versus frequency or using the shear viscoelastic parameters of the skin [6], [7]. For instance, variations in wave velocity according to body region [8] and the age of the subject [9]–[11] have been reported. However, as the skin is made up of three principle layers—namely the epidermis, dermis, and hypodermis—some 50  $\mu\text{m}$ , 1 mm, and several millimeters thick, respectively, which can vary depending on the location within the body, such an approach would prove difficult in terms of recovering the intrinsic mechanical properties of each layer independently.

The goal of this paper is to propose a new, noninvasive approach allowing local Young's modulus to be recovered in the dermis. The first step consists in adapting the transient elastography technique devoted to centimeter-sized media—such as muscle, breast, or liver—to millimeter-sized media such as the skin. The second step consists in assessing the suitability of the method by numerical simulation. During the final stage, experimental results were recorded in skin-mimicking phantoms and *in vivo* on the human forearm of healthy volunteers.

## II. FROM TRANSIENT ELASTOGRAPHY TO SKIN SONOELASTOGRAPHY

### A. Adaptation of the Shear Elasticity Probe

A new elasticity assessment method using volumic shear wave propagation has been developed over the last 5 years. This is known as transient elastography [12]–[15], which was inspired by the sonoelastography technique [16]–[18]. Transient elastography is based on the combination of an ultrafast echographic device, which detects and follows the propagation of shear waves generated by a mechanical vibrating system. From the speckle motion induced by a low-frequency, pulsed vibration (100–500 Hz) applied by

Manuscript received October 27, 2003; accepted March 30, 2004.

J.-L. Gennisson, M. Tanter, S. Catheline, M. Fink, and L. Sandrin are with the Laboratoire Ondes et Acoustique, Ecole Supérieure de Physique et de Chimie Industrielle de la Ville de Paris, Université Denis Diderot Paris VII, Unité Mixte de Recherche Centre National de la Recherche Scientifique (UMR CNRS) 7587, 75231 Paris, Cedex 05, France (e-mail: michael.tanter@espci.fr).

T. Baldeweck, C. Cornillon, and B. Querleux are with L'Oreal-Recherche, 93601 Aulnay sous bois, France.

the front face of the transducer itself, the backscattered echoes recorded from the medium are used to deduce tissue displacements using a classical speckle cross-correlation algorithm [19]. Shear wave velocity then is recovered with phase analysis of the displacements field at the central frequency. As Young's modulus is directly related to the shear elastic modulus in soft tissues,  $E \approx 3\mu = 3\rho V_S^2$  [20], where  $E$ ,  $\mu$ ,  $\rho$ ,  $V_S$  are the Young's modulus, the shear modulus (Lamé's coefficients), the density and the shear wave velocity, respectively, transient elastography facilitates determination of the local elastic properties of centimeter-sized soft media such as muscle, liver, or breast.

Adaptation of this technique to skin investigation poses a challenge as shear elasticity will have to be measured in a layer of about a few millimeters. Moreover, some shear elasticity measurements attribute a very strong Young's modulus of the order of 1 MPa to the skin [21]–[23]. Thus, the shear wave velocity is roughly 30 m/s in the dermis ( $E \approx 3\rho V_S^2$ ). When transient vibration is used, the ultrasonic pulse repetition frequency (PRF) should be at least 200 kHz if shear wave propagation is to be followed every tenth of a millimeter. Such a PRF is not applicable, and the transposition of transient elastography from muscle or liver applications to the skin should prove difficult and should, at least call for an ultrasound transducer with a highly specific design. One solution is to use a steady-state (sonoelastography) instead of a transient (transient elastography) vibration. If a monochromatic vibration in the 300 Hz range is applied, the shear viscosity is sufficiently strong to prevent reflected shear waves from returning from deeper soft layers (such as muscles), one of the main drawbacks of sonoelastography. Moreover, to follow shear wave propagation every tenth of a millimeter, shear wave-induced motion can be stroboscoped using a high number of low-frequency periods, until a limit value that was found experimentally equal to 30, and choosing a reasonable ultrasonic PRF (2 kHz). Consequently, the shear wave speed is much more precise because it is based on synchronous detection.

Regarding the mechanical design of the hand-held probe, it would have been more convenient to apply the low-frequency vibration using the front face of the transducer itself. However, transducer motion has to be measured precisely and taken into account in such cases in order to recover only those tissue displacements induced by the vibration in the referential of the ultrasonic probe [14]. This can easily be achieved for experiments on muscle, breast, or liver by tracking the transducer displacements on fixed targets in the human body. However, it is very difficult in skin experiments. Therefore, we decided to separate mechanically the ultrasonic probe and the low-frequency vibrator. For a compact and easy-to-use system, the low-frequency shear wave, thus, is generated by an independent ring surrounding the ultrasound transducer.

### B. A New Elasticity Probe for the Skin

This concept is applied by developing a convenient hand-held probe dedicated to skin elasticity assessment.

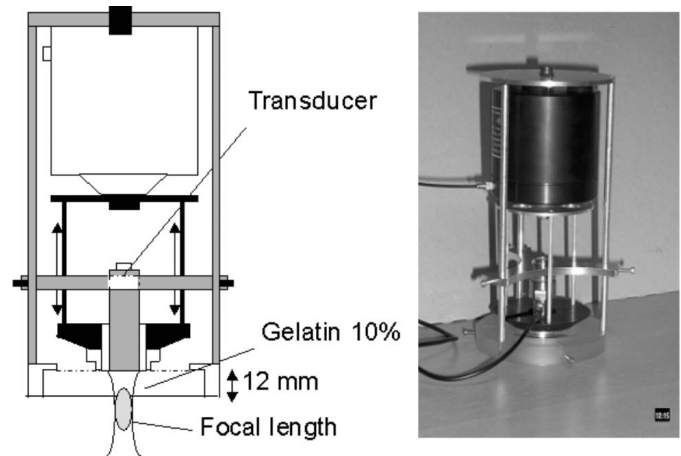


Fig. 1. The new shear probe for skin elastography. The ultrasonic transducer is fixed to a frame attached to the vibrator. The ring, which is entirely separate from the transducer, vibrates on the surface of a gelatin disc. A gelatin-coupling layer is used to locate the ultrasonic focal distance at the skin surface. The moving part is highlighted in black and the fixed section is in gray, including the transducer.

The experimental setup is shown in Fig. 1. The probe comprises a 50 MHz (Panametrics, 50 MHz-12mm, La Garenne Colombe, France) focused transducer with a focal length of 12 mm surrounded by an 18 mm ring mounted on a vibrator (Brüel & Kjaer, mini shaker no 4810, Aerum, Denmark). The transducer is maintained at the center of the ring by means of a metallic structure fixed to the back of the vibrator and mechanically dissociated from the ring, such that the vibration induced by the ring does not affect the ultrasonic transducer.

The ring is excited by a function generator (Agilent 33120A, France) and produces a 300 Hz sinusoidal shear wave. As a coupling medium, 10% gelatin concentration, 12 mm high, is used in order to place the ultrasonic focal spot exactly on the skin surface and to ensure good shear wave transmission.

By using a ring vibrator of this type, the shear waves can be focused on the ultrasonic beam axis at the focal length of the transducer [Fig. 2(a)]. In fact, the direction of shear waves generated by a point source in a semi-infinite medium at 300 Hz frequency presents side lobes at  $35^\circ$ . The angular direction pattern is calculated with numerical simulation based on the impulse diffraction theory in an isotropic infinite medium and is presented on Fig. 2(b) [24]. The computation parameters in typical soft tissues are  $1100 \text{ kg/m}^3$ , 2.47 GPa, and 10 kPa in terms of density, bulk, and shear elasticities, respectively [23]. According to the Huygens principle, the ring is divided into a multitude of point sources. The side lobes generated by each point source constructively affect the ultrasonic beam axis. Thus, with a correctly designed ring, it is possible to focus the shear wave on the ultrasonic beam axis at the focal length of the transducer [Fig. 2(a)] [25].

As shear waves are focused on the ultrasonic beam axis, their energy is increased in the focal area of the transducer.

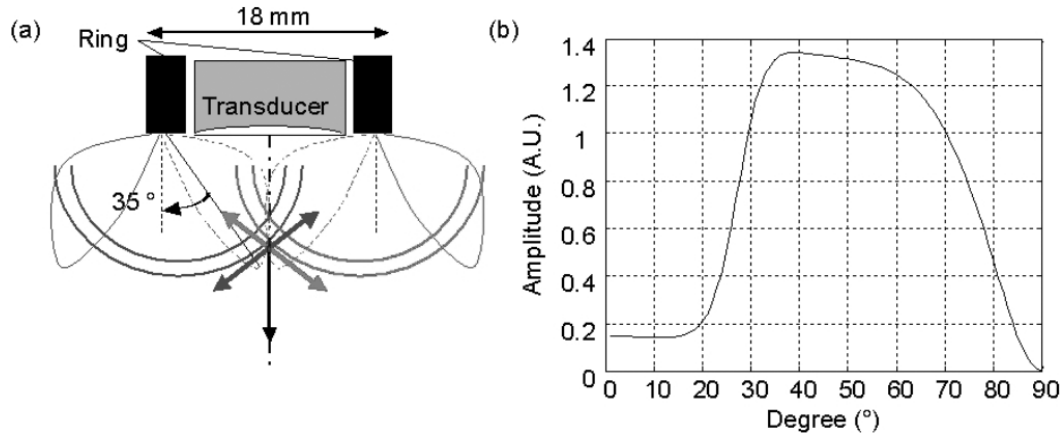


Fig. 2. (a) Diagram of the ring around the transducer. The ring focuses the shear waves on the ultrasonic beam. (b) Shear wave side lobe computed with impulse diffraction theory in an isotropic infinite medium, 12 mm from a point source. Maximum energy is directed at 35°.

In a homogeneous medium, the maximum local displacement induced by a piston source vibrating at the surface of a medium [Fig. 3(a)], as in transient elastography with the shear elasticity probe, is compared to the maximum local displacement induced by a ring in the same configuration [Fig. 3(b)]. The piston and the ring have the same surface and diameters of 7 mm (the shear elasticity probe transducer diameter) and 18 mm external diameter (the minimum size for a ring surrounding the 50 MHz focused transducer), respectively. The amplitude of the shear wave is increased by 3 dB in the ultrasonic focal zone of the transducer at 12 mm on the ultrasonic axis by the shear-focusing pattern induced by the ring [Fig. 3(c)].

This ring-shaped vibrating system is particularly suitable for estimating skin elasticity because it tends to increase tissue displacements due to shear vibrations at the desired location.

Regarding the ultrasonic component, the transducer is stimulated by a 200 MHz pulser/receiver (Panametrics 5900PR) and each radio frequency (RF) A-scan (back-scattered echoes) line is digitized at a 500 MHz sampling frequency by a peripheral component interconnect (PCI) digitizer (Acquis DP210, Monroe, NY) and recorded on a personal computer. The 200 RF signals (A-scan) can be stored with a recurrence frequency of 2 kHz.

### C. Validation of the Sonoelastography Technique by Numerical Simulation

Shear wave propagation in three thin layers was simulated using two-dimensional (2-D) finite difference simulation of the wave propagation in viscoelastic solids developed by M. Tanter<sup>1</sup>. This simulation computes the action of two point forces with symmetric conditions along the symmetry axis between both sources. The three simulated layers are (Fig. 4): the gelatin disc (12 mm thick due to the ultrasonic focal length), the dermis (about 2 mm thick), and the upper part of the hypodermis (about 3 mm thick).

The simulation parameters in the dermis and hypodermis are fixed from results found in the literature [21]–[23]. Thus, shear wave speeds of 3 m/s, 30 m/s, and 3 m/s are recorded for each respective layer.

As the shear wavelength is much bigger than the ring section ( $\lambda_S \approx 10$  mm in the gelatin layer, the ring is 1.5 mm in width), the ring action can be simulated by two point sources. The simulation mesh is defined by the following boundary conditions: absorption on the sides and fixed boundary conditions at a depth of 0 and 30 mm (Fig. 4). The other parameters are 1100 kg/m<sup>3</sup> for the density, and the longitudinal wave speed is 10 times higher than the shear wave speed in the dermis for each layer, which corresponds to a bulk modulus of the order of 0.1 GPa, and a wavelength huge in comparison with the grid dimensions.

The longitudinal displacements field  $u_z(x, z, t)$  induced by the ring vibrations is presented at different phases in Fig. 5. The shear wave speed subsequently is estimated at the central frequency (300 Hz) along the ultrasonic axis (Fig. 5). The Fourier transformation of the temporal displacement field at each depth allows the phase delay to be estimated at the 300 Hz vibrating frequency versus depth and thus facilitates recovery of the shear wave speed.

The low-frequency wave-phase delay is plotted at the central frequency as a function of depth in Fig. 6. The three layers are perfectly visible, and the low-frequency wave velocity is estimated by linear regression in two different zones, 12 to 13.8 mm and 13.8 to 20 mm corresponding to the simulated dermis and hypodermis, respectively.

A comparison of the velocities injected in the numerical simulation and the estimated velocities estimated is presented in Table I. The standard deviation is given from the linear fit of the different phase delay-versus-time.

As expected, the slope of the phase delay is strong in the layers in which the shear velocity is slow (gelatin and hypodermis) and low in the layer in which the shear velocity is fast (dermis). In addition, the shape of the phase is always the same with three different zones corresponding to the three different layers, regardless of the simulated

<sup>1</sup>ACEL: Finite difference simulation of the ACoustic and ELastic waves equations, <http://www.loa.espci.fr>.

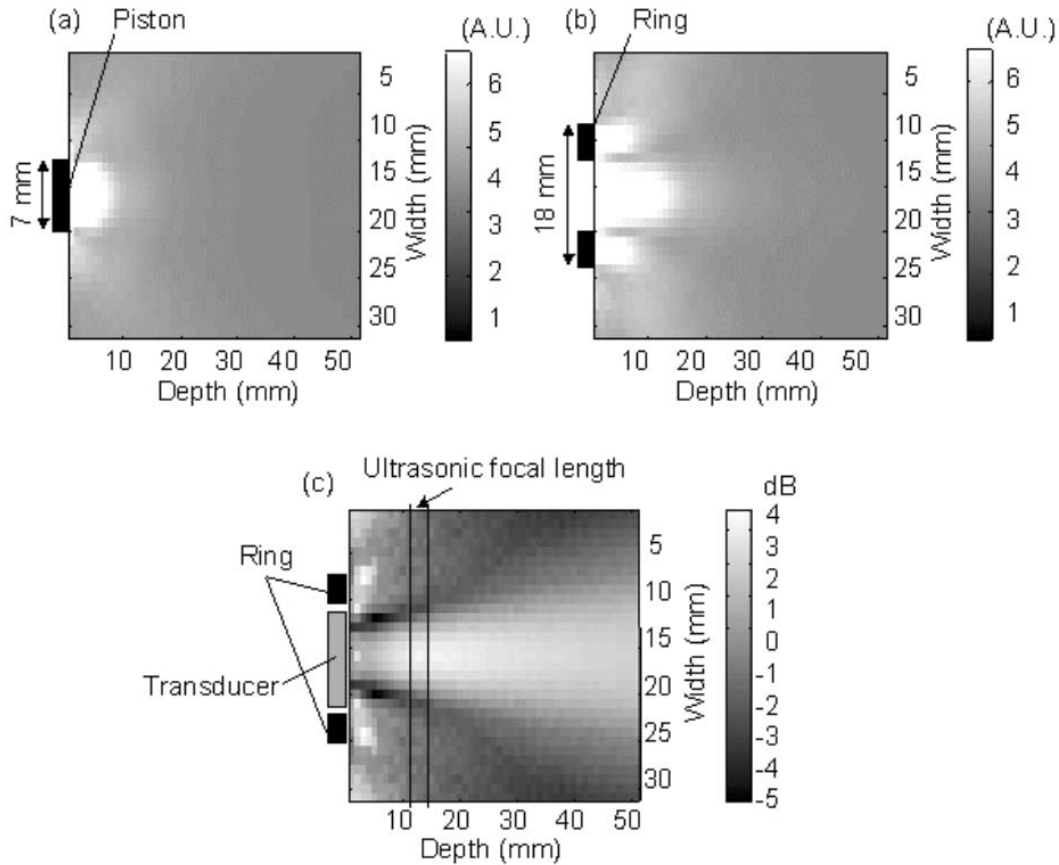


Fig. 3. (a) and (b) Amplitude of the displacement field of the shear wave in the spectral domain, of a piston source, and of a ring source at central frequency. (c) Increase in decibels between a ring with an external diameter of 18 mm and a piston with the same surface. The energy of the shear wave is increased on the ultrasonic beam axis.

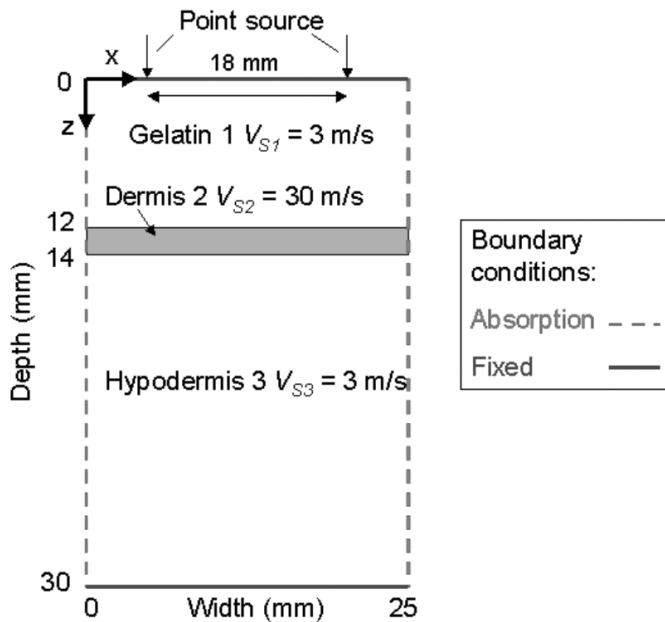


Fig. 4. Parameters used in the numerical simulation. The shear wave speed distribution is heterogeneous, and the longitudinal wave speed is homogeneous in the three layers. The mesh grid comprises  $250 \times 300$  points.

TABLE I  
COMPARISON BETWEEN THEORETICAL AND ESTIMATED SIMULATION VELOCITIES.

Zone	Theoretical velocities (m/s)	Estimated velocities (m/s)
Simulated Dermis	15	$33 \pm 1$
	30	$57 \pm 2$
	60	$101 \pm 6$
Simulated Hypodermis	1.5	$9 \pm 1$
	3	$13 \pm 1$
	6	$21 \pm 1$

parameters. The low-frequency wave velocities estimated from one layer to the other vary in the same order of magnitude.

Nevertheless, the shear wave velocities are overestimated compared to the simulated values. This result can be justified by the following assumptions. In this particular application, it is impossible to dissociate the displacements due to the longitudinal waves and the shear waves in the very near field of the interfaces as the medium vibrates at steady state, unlike the situation in transient elastography. Moreover, some reflections on the different layers can influence the velocity estimation in the three zones.

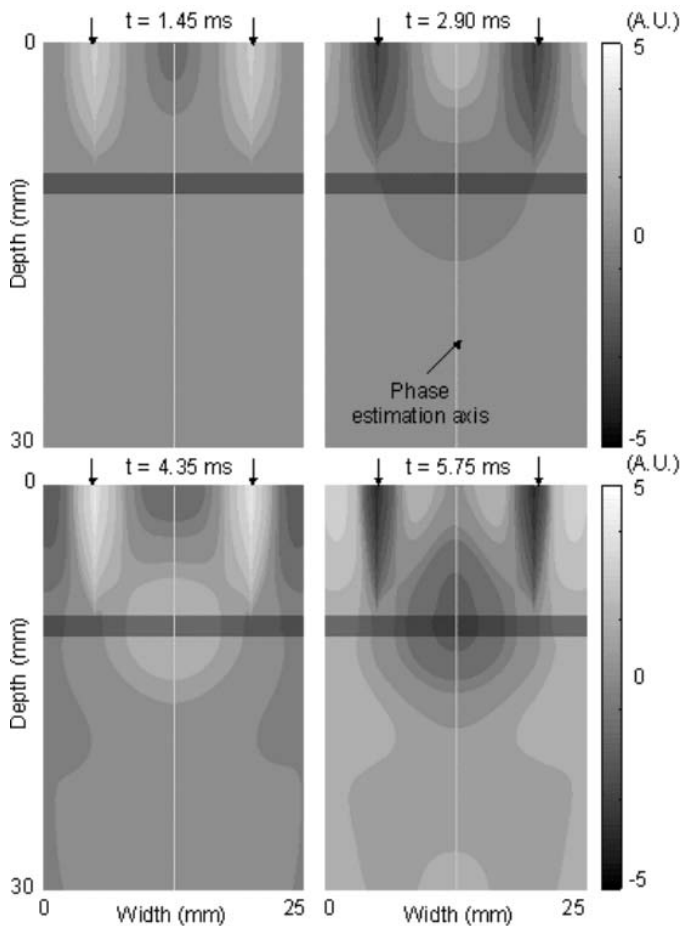


Fig. 5. Amplitude of the displacement field of the shear wave generated by two point sources (symbolized by two arrows) at different phases. The boundary conditions are: absorption on the sides and fixed boundary conditions at a depth of 0 and 30 mm. The shear wave phase delay is calculated at the central frequency on the axis, located on the 12.5 mm abscissa.

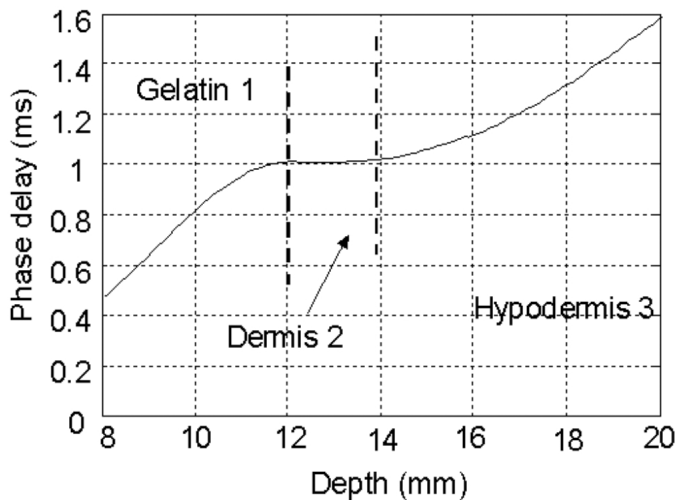


Fig. 6. Phase delay of the low-frequency wave as a function of depth computed by finite difference simulation. The three simulated layers are perfectly visible. The low-frequency wave velocities are estimated by linear regression in different zones for the dermis and hypodermis.

Because the diffraction effects play an important role [26], the shear wave speeds are overestimated in the near field of each interface.

In the initial gelatin layer, the phase delay becomes linear after 8 mm. This is due to near-field diffraction effects because the shear wavelength is comparable to the size of the layer ( $\lambda_{S1} \approx 10$  mm). In the dermis, the shear wavelength increases ( $\lambda_{S2} \approx 100$  mm). Shear wave velocity is estimated again in a near-field zone. From another point of view, the incident shear wave operates as a new low-frequency source on the surface of the dermis due to mode conversion. This overestimation is corroborated in the hypodermis as the same effects are present.

Thus, shear wave velocity is overvalued in the three layers. According to the simulation, the ratio between the estimated velocity and the true shear wave velocity in free space is roughly factor 2 in the dermis and factor 5 in the hypodermis. The true shear wave velocity cannot be recovered in a quantitative manner without taking into account diffraction corrections. Such diffraction biases can be corrected using a numerical simulation dedicated to this problem, taking into account the different layers and the considerable difference in velocity of the longitudinal and the shear waves. Thus, a table of diffraction correction factors can be built using simulations taking into account a complete range of skin stiffness, and this table can be applied to experimental data. Even without taking into account such a precise correction table, estimated velocities, however, are proportional to the true shear velocities. For that reason, a local parameter of each layer already can be assessed in relation to its elasticity. The next part of this paper focuses on estimated elasticities, taking into account the correction factors on the calculated velocities. The feasibility of such a method is verified by an experimental approach to skin-mimicking phantoms.

### III. RESULTS

#### A. Preliminary Tests on Agar-Gelatin Phantoms

To establish the validity of our new probe, preliminary tests were performed on 5-mm thick Agar-gelatin phantoms. The measurements were recorded in a phantom of 15% concentrated gelatin and 5% concentrated Agar. The Agar powder is used as ultrasonic scatterers, and the gelatin is used as a suspending medium. The A-scan presented in Fig. 7(a) corresponds to one of the 200 RF signals stored in the channel memory at a 2 kHz repetition rate. It is divided into three zones corresponding to the gelatin disc, the thin layer mimicking the skin and the phantom backup. The longitudinal displacements field  $u_z(x, z, t)$  is recovered by correlating the successive A-scans stored in the memory [Fig. 7(b)]. The three zones are visible on the gray level image of the displacements amplitude at each depth as a function of time.

The dependence of the phase delay of the low-frequency wave versus depth can be evaluated by analyzing the

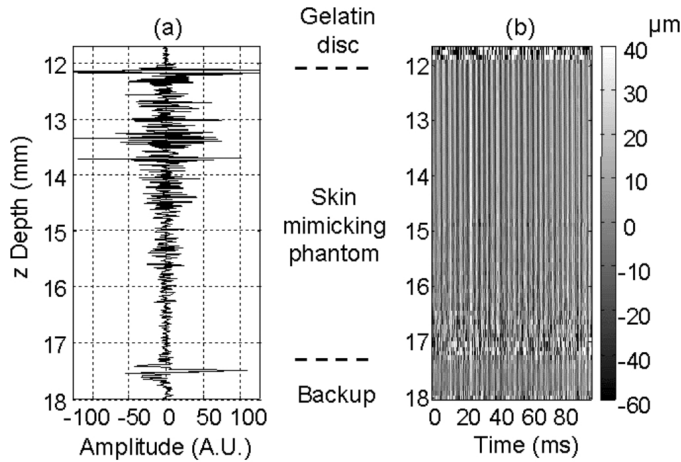


Fig. 7. (a) One of the 200 A-scans stored in the channel memory corresponding to the skin-mimicking phantom as a function of depth. (b) Displacements field in the phantom along the depth-versus-time axis obtained by cross correlation on the successive A-scans.

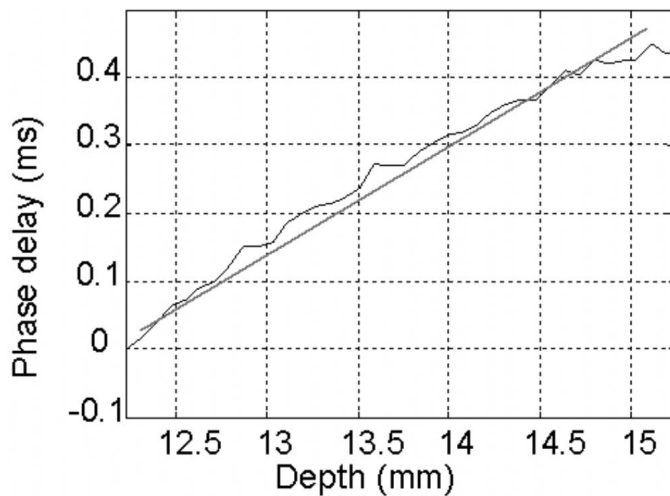


Fig. 8. Phase delay of the low-frequency wave in a thin phantom versus depth. Velocity is found to be  $6.00 \pm 0.73$  m/s, using a linear fit.

Fourier transformation of the longitudinal displacements field  $u_z(x, z, t)$  at the central frequency of the vibration (300 Hz) (Fig. 8). The slope of the phase delay is obtained by linear regression, and the error is estimated by standard deviation. This yields a speed of  $6.00 \pm 0.73$  m/s for the low-frequency wave in the medium over the first 3 mm.

Changes in the velocity of the low-frequency wave with the number of acquisitions can be considered in terms of reproducibility. Fig. 9 presents the results corresponding to 25 successive acquisitions on the phantom and, hence, to 25 independent phase-delay laws. The 25 acquisitions were chosen to provide a good reduction in measurement variance and to preserve a reasonable *in vivo* experimentation time of about 12 s for a time interval equal to 0.5 s between each acquisition.

The mean value of these 25 acquisitions now can be calculated using two different approaches. Either the mean

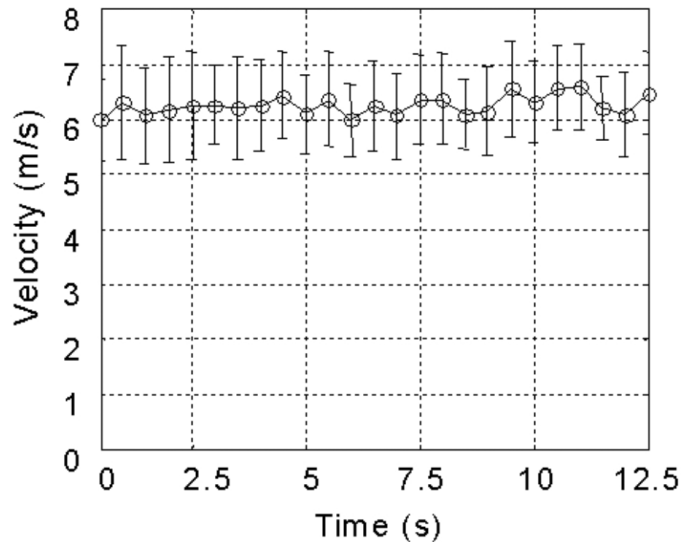


Fig. 9. Reproducibility test of the low-frequency wave velocity estimation regarding the number of acquisitions.

value and the standard deviation of the 25 final velocity values are evaluated or the mean phase is calculated from the 25 phase-delay laws versus depth acquired, and the velocity and standard deviation are estimated from this mean phase-delay law.

In the first case, the low-frequency velocity has a mean value of  $\bar{V}_{LF1} = 6.30 \pm 0.19$  m/s. The standard deviation  $\Delta V_{LF1}$  is an indicator of the scattering of the 25 acquisitions. In fact, this method does not estimate the linearity between the depth and the phase delay but provides information about the reproducibility of the velocity estimation. Despite the fact that the low-frequency wave speed is overvalued, this standard deviation confirms the good reproducibility of the technique.

In the second case, the mean value is:  $\bar{V}_{LF2} = 6.29 \pm 0.13$  m/s. The error estimation  $\Delta V_{LF2}$  on the mean phase with linear regression is more relevant as it corresponds to the relative error on the low-frequency wave velocity (see Appendix). Thus, the mean value  $\bar{V}_{LF2}$  of the low-frequency wave velocity for 25 acquisitions always will be considered in the following experiments.

### B. Comparison Between Different Phantoms

The low-frequency wave velocity was estimated on four different Agar-gelatin skin phantoms (5 mm thick). The elasticity was increased by changing the gelatin concentration, and the same Agar concentration was used for all phantoms (3%). A set of 25 acquisitions was made for each phantom (Fig. 10). The mean velocity values were  $2.51 \pm 0.11$  m/s,  $4.58 \pm 0.09$  m/s,  $7.58 \pm 0.56$  m/s, and  $10.20 \pm 0.35$  m/s, respectively, for the phantoms with 10%, 15%, 20%, and 25% concentrated gelatin.

As expected, the low-frequency wave velocity increases with the gelatin concentration as the phantom elasticity increases with gelatin concentration. Elastic properties from 1.73 to 28.61 kPa, taking into account the diffraction factor

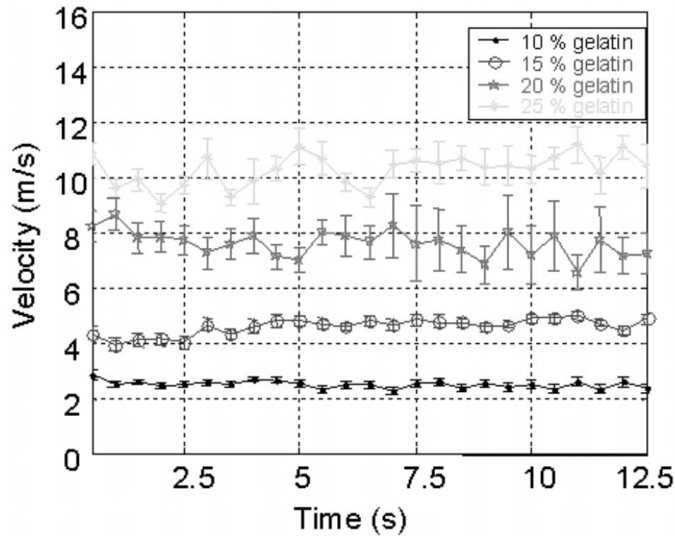


Fig. 10. Low-frequency wave speed versus acquisition number (i.e., time) on four different phantoms. The mean velocity values are  $2.51 \pm 0.11$  m/s,  $4.58 \pm 0.09$  m/s,  $7.58 \pm 0.56$  m/s, and  $10.20 \pm 0.35$  m/s, respectively, for the 10%, 15%, 20%, and 25% gelatin-concentrated phantom.

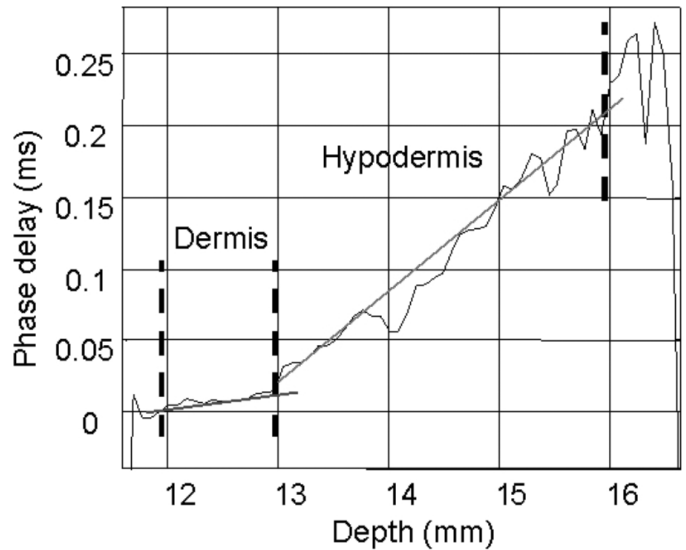


Fig. 12. Phase delay of the low-frequency wave in the skin versus depth. Two zones corresponding to the dermis and the hypodermis can be distinguished clearly, with uncorrected velocities of  $V_D = 85.04 \pm 11.13$  m/s and  $V_H = 14.84 \pm 0.41$  m/s, respectively. After diffraction corrections to the velocities, the corresponding elasticities are 1.98 MPa and 9.68 kPa, respectively.

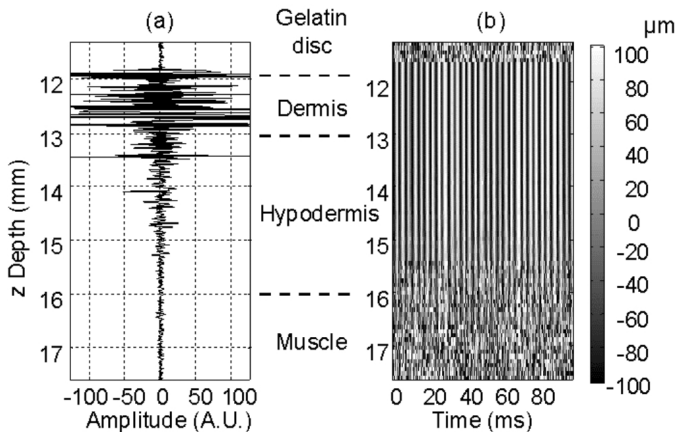


Fig. 11. (a) One of the 200 A-scans obtained on the forearm skin of an adult female as a function of depth. The three principle layers are visible: the gelatin, the dermis, and the hypodermis. (b) The gray-colored displacements field in adult female forearm skin along the ultrasonic beam versus time axis.

of 2 on the velocities, are differentiated in all phantoms. These results obtained in phantoms a few millimeters thick are in good agreement with other results recorded with other methods in phantoms of the same gelatin concentration and a few centimeters thick [14], [27].

### C. In-Vivo Experiments

Fig. 11 shows a typical ultrasonic A-scan signal of the skin of a healthy young subject [Fig. 11(a)] and the displacement field of the low-frequency wave as a function of time [Fig. 11(b)]. Four different zones are visible on the A-scan, the first from the beginning to 11.8 mm corresponds to the gelatin disc in front of the system, the second from 11.8 mm to 13.1 mm corresponds to the skin, the third as

far as approximately 16 mm corresponds to the hypodermis, and the muscle. In the case of the latter, it is difficult to define the exact position of the muscle-hypodermis boundary because the signal-to-noise ratio is weaker at such a high 50 MHz frequency. The quality of the speckle is very good in the other zones. There is a strong signal-to-noise ratio, and the experimental displacements field is clean. This allows accurate estimation of the phase delay.

A set of 25 acquisitions is recorded in this subject, and the mean phase is presented in Fig. 12. Two zones of different velocities corresponding to the dermis and the hypodermis can be distinguished clearly. The velocities are found to be  $V_D = 85.04 \pm 11.13$  m/s in the dermis (1.05 mm thick) and  $V_H = 14.84 \pm 0.41$  m/s in the hypodermis (2.86 mm thick). The thickness measured via the phase-delay law is in good agreement with the thickness deduced from the A-scan signal of Fig. 11(a).

Low-frequency speeds from other experiments are presented for four subjects in Table II. These values range from 66.27 to 106.31 m/s in the dermis and 8.35 to 14.84 m/s in the hypodermis. Considering correction factors of 2 and 5 for dermal and hypodermal velocities due to diffraction biases, the corresponding shear modulus ranges from 1.20 to 3.10 MPa in the dermis and 3.10 to 9.68 kPa in the hypodermis. The results are in good agreement with the literature [21]–[23]. The shape of the phase delay is always the same as in Fig. 12 for each subject. A significant difference between the velocities in the two layers was noticed in each subject. The mean velocity is found to be  $83.89 \pm 15.17$  m/s in the dermis and  $10.88 \pm 2.70$  m/s in the hypodermis. The mean thickness of the two layers is  $1.14 \pm 0.20$  mm and  $1.59 \pm 0.79$  mm, respectively.

TABLE II  
LOW-FREQUENCY WAVE VELOCITIES, ELASTICITIES AND THICKNESS IN THE FOREARM DERMIS AND HYPODERMIS.

Subject	Dermis shear velocity (m/s)	Dermis shear elasticity $\mu_D$ (MPa)	Dermis thickness (mm)	Hypodermis shear velocity (m/s)	Hypodermis shear elasticity $\mu_H$ (kPa)	Hypodermis thickness (mm)
1	74.24 $\pm$ 14.75	1.51	1.13	8.40 $\pm$ 0.31	3.10	1.67
2	85.04 $\pm$ 11.13	1.98	1.05	14.84 $\pm$ 0.41	9.68	2.86
3	106.31 $\pm$ 35.86	3.10	0.89	12.30 $\pm$ 1.63	6.65	1.08
4	66.27 $\pm$ 15.49	1.20	1.23	8.63 $\pm$ 1.03	3.25	0.79
5	87.63 $\pm$ 5.69	2.11	1.43	10.25 $\pm$ 0.29	4.62	1.57

#### IV. CONCLUSIONS

A noninvasive ultrasound-based probe for the assessment of human skin elasticity was proposed. The shear elasticity estimation is based on the sonoelastography technique and has been adapted to take into account the specificity of millimeter-thin layers like human skin. The shear wave velocity of the skin *in vivo* changed with depth through the different layers. The layer corresponding to the dermis was seen to have a higher velocity than that in the hypodermis.

This study presents the first *in vivo* application of sonoelastography to characterize the skin. Measurements within the dermis are not corrupted by the influence of the stratum corneum, epidermis, or hypodermis; and they correspond to a local and intrinsic parameter that is not influenced by the thickness of the different skin layers. Consequently, such a method, for instance, will be particularly interesting for improving our knowledge of dermal alterations induced by the aging processes of the skin.

#### APPENDIX A

The point  $t_i$  (phase delay) versus  $x_i$  (depth) couple is set around a line of slope  $a$  with some random difference  $e_i$ , so:

$$t_i = ax_i + b + e_i. \quad (1)$$

We suppose that the difference  $e_i$  is random with a mean value equal to zero, not two-two correlate and with a standard deviation  $\sigma_e$ . The following mean value is observed:

$$\bar{x} = \frac{1}{n} \sum_{i=1}^n x_i, \quad \bar{t} = \frac{1}{n} \sum_{i=1}^n t_i, \quad \bar{e} = \frac{1}{n} \sum_{i=1}^n e_i. \quad (2)$$

The least square method gives us an estimation  $\hat{a}$  of the slope  $a$ :

$$\hat{a} = \frac{\sum_{i=1}^n (x_i - \bar{x})(t_i - \bar{t})}{\sum_{i=1}^n (x_i - \bar{x})^2}. \quad (3)$$

This estimation  $\hat{a}$  has a random variation due only to  $t_i$  (phase delay) because the depth  $x_i$  is very specific. The problem lies in investigating its mean value and variance.

- The mean value of  $\hat{a}$ :

$$\langle \hat{a} \rangle = \frac{\sum_{i=1}^n (x_i - \bar{x}) \langle (t_i - \bar{t}) \rangle}{\sum_{i=1}^n (x_i - \bar{x})^2}, \quad (4)$$

but if the mean value of  $e_i$  is zero:

$$\langle (t_i - \bar{t}) \rangle = a(x_i - \bar{x}) + \langle e_i \rangle - \langle \bar{e} \rangle = a(x_i - \bar{x}). \quad (5)$$

So  $\langle \hat{a} \rangle = a$  and the estimation of  $a$  is noise-free.

- The variance of  $\hat{a}$ :

We rewrite  $\hat{a}$  as follows:

$$\hat{a} = a + \frac{\sum_{i=1}^n (x_i - \bar{x})(e_i - \bar{e})}{\sum_{i=1}^n (x_i - \bar{x})^2}. \quad (6)$$

So the variance of  $\hat{a}$  is the variance of  $T$ :

$$\begin{aligned} \text{Var}(T) &= \frac{\sum_{j=1}^n \sum_{i=1}^n (x_i - \bar{x})(x_j - \bar{x}) \langle (e_i - \bar{e})(e_j - \bar{e}) \rangle}{\left[ \sum_{i=1}^n (x_i - \bar{x})^2 \right]^2}, \\ &= a + T \end{aligned} \quad (7)$$

with

$$\langle (e_i - \bar{e})(e_j - \bar{e}) \rangle = \sigma_e^2 \delta_{ij} - \frac{1}{n} \sigma_e^2. \quad (8)$$

As the  $x_i$  are very specific ( $x_i = i\delta x$ ):

$$\sum_{i=1}^n (x_i - \bar{x}) = 0, \quad (9)$$

and

$$\sum_{i=1}^n (x_i - \bar{x})^2 = \frac{\delta x^2}{12} n(n+1)(n-1). \quad (10)$$

So the variance of  $\hat{a}$  is:

$$\text{Var}(\hat{a}) = \frac{12\sigma_e^2}{\delta x^2 n(n+1)(n-1)}, \quad (11)$$

with

$$\sigma_e = \sqrt{\frac{\sum_{i=1}^n (t_i - ax_i - b)^2}{n}}. \quad (12)$$

Thus the slowness error is given by:

$$\Delta a = \sqrt{\text{Var}(\hat{a})} = \frac{2\sqrt{3}}{\delta x \sqrt{n(n+1)(n-1)}} \sigma_e. \quad (13)$$

In terms of velocity, if  $\Delta a \ll a$ ,  $\Delta v/v = \Delta a/a$ .

#### ACKNOWLEDGMENT

We would like to thank Arnaud Derode and Didier Cassereau for their expert assistance in signal processing and numerical simulation.

#### REFERENCES

- [1] P. G. Agache, C. Monneur, J.-L. Leveque, and J. De Rigal, "Mechanical properties and Young's modulus of human skin," *Arch. Dermatol. Res.*, vol. 269, pp. 221–232, 1980.
- [2] J. S. Comaish, P. R. H. Harborow, and D. A. Hofman, "A hand held friction meter," *Brit. J. Dermatol.*, vol. 89, pp. 33–50, 1973.
- [3] A. O. Barel, W. Courage, and P. Clarys, "Suction method for measurement of skin mechanical properties: The cutometer," in *Handbook of Non-Invasive Methods and the Skin*. J. Serup and G. Jemec, Eds. London: CRC Press, 1995, pp. 335–339.
- [4] G. E. Piérard and C. M. Lapière, "Physiopathological variations in the mechanical properties of skin," *Arch. Dermatol. Res.*, vol. 260, pp. 313–329, 1977.
- [5] H. Tronnier and H. H. Wagnener, "Ueber die frequenz leitfähigkeit der menschlichen haut," *Dermatologica*, vol. 104, pp. 135–142, 1952.
- [6] P. L. Dorogi, G. M. Dewitt, B. R. Stone, and E. M. Buras, "Viscoelasticity of skin in vivo using shear wave propagation," *Bioeng. Skin*, vol. 2, pp. 59–70, 1986.
- [7] J. Pereira, J. M. Mansour, and B. R. Davis, "Analysis of shear wave propagation in skin: Application to an experimental procedure," *J. Biomech.*, vol. 23, pp. 745–751, 1990.
- [8] R. M. Dahlgren and W. H. Elsna, "Measurement of skin condition by sonic velocity," *J. Soc. Cosmet. Chem.*, vol. 35, pp. 1–19, 1984.
- [9] R. O. Potts, D. A. Chrisman, and E. M. Buras, "The dynamic mechanical properties of human skin in vivo," *J. Biomech.*, vol. 16, pp. 365–372, 1983.
- [10] B. R. Davis, E. Bahniuk, J. K. Young, C. M. Barnard, and J. M. Mansour, "Age dependent change in the shear wave propagation through human skin," *J. Expr. Gerontol.*, vol. 24, pp. 201–210, 1989.
- [11] J. Pereira, J. M. Mansour, and B. R. Davis, "The effect of layer properties on shear disturbance propagation in skin," *J. Biomech. Eng.*, vol. 113, pp. 30–35, 1991.
- [12] S. Catheline, J. L. Thomas, F. Wu, and M. Fink, "Diffraction field of a low frequency vibrator in soft tissues using transient elastography," *IEEE Trans. Ultrason., Ferroelect., Freq. Contr.*, vol. 46, no. 4, pp. 1013–1019, 1999.
- [13] L. Sandrin, S. Catheline, M. Tanter, X. Hennequin, and M. Fink, "Time resolved pulsed elastography with ultrafast ultrasonic imaging," *Ultrason. Imag.*, vol. 21, no. 4, pp. 259–272, 1999.
- [14] L. Sandrin, M. Tanter, J. L. Gennisson, S. Catheline, and M. Fink, "Shear elasticity probe for soft tissues with 1D transient elastography," *IEEE Trans. Ultrason., Ferroelect., Freq. Contr.*, vol. 49, no. 4, pp. 436–446, 2002.
- [15] L. Sandrin, M. Tanter, S. Catheline, and M. Fink, "Shear modulus imaging using 2D transient elastography," *IEEE Trans. Ultrason., Ferroelect., Freq. Contr.*, vol. 49, no. 4, pp. 426–435, 2002.
- [16] R. M. Lerner, K. J. Parker, J. Holen, R. Gramiak, and R. C. Waag, "Sonoelasticity: Medical elasticity images derived from ultrasound signals in mechanically vibrated target," *Acoust. Imaging*, vol. 16, pp. 317–327, 1987.
- [17] S. F. Levinson, M. Shinagawa, and T. Sato, "Sonoelastic determination of human skeletal muscle elasticity," *J. Biomech.*, vol. 28, no. 10, pp. 1145–1154, 1995.
- [18] V. Dutt, R. R. Kinnick, and J. F. Greenleaf, "Acoustic shear wave displacement measurement using ultrasound," in *Proc. IEEE Ultrason. Symp.*, vol. 2, 1996, pp. 1185–1188.
- [19] J. Ophir, E. Céspedes, H. Ponnekanti, Y. Yasdi, and X. Li, "Elastography: A quantitative method for imaging the elasticity of biological tissues," *Ultrason. Imag.*, vol. 13, pp. 111–134, 1991.
- [20] E. Dieulesaint and D. Royer, *Elastic Waves in Solids*. 1 ed. Springer, 1995.
- [21] R. Grahame, "Elasticity of human skin in vivo," *Ann. Phys. Med.*, vol. 10, pp. 130–134, 1969.
- [22] C. Escoffier, J. de Rigal, A. Rochefort, R. Vasselet, J.-L. Leveque, and P. G. Agache, "Age related mechanical properties of human skin: An in vivo study," *J. Invest. Dermatol.*, vol. 93, pp. 353–357, 1989.
- [23] A. P. Sarvazyan, O. V. Rudenko, S. D. Swanson, J. B. Fowlkes, and S. Y. Emelianov, "Shear wave elasticity imaging: A new ultrasonic technology of medical diagnostics," *Ultrasound Med. Biol.*, vol. 24, no. 9, pp. 1419–1435, 1998.
- [24] D. Cassereau and D. Guyomar, "Computation of the impulse diffraction of any obstacle by impulse ray modeling—Prediction of the signal distortions," *J. Acoust. Soc. Amer.*, vol. 84, no. 4, pp. 1504–1516, 1988.
- [25] Z. Wu, L. S. Taylor, D. J. Rubens, and K. J. Parker, "Shear wave focusing for three-dimensional sonoelastography," *J. Acoust. Soc. Amer.*, vol. 111, no. 1, pp. 439–446, 2002.
- [26] S. Catheline, F. Wu, and M. Fink, "A solution to diffraction biases in sonoelasticity: The acoustic impulse technique," *J. Acoust. Soc. Amer.*, vol. 105, no. 5, pp. 2941–2950, 1999.
- [27] V. Dutt, R. R. Kinnick, R. Muthupillai, T. E. Oliphant, R. L. Ehman, and J. F. Greenleaf, "Acoustic shear-wave imaging using echo ultrasound compared to magnetic resonance elastography," *Ultrasound Med. Biol.*, vol. 26, no. 3, pp. 397–403, 2000.



**Jean-Luc Gennisson** was born in June 1974 in Paris, France. He received the D.E.A. degree in Electronics in 2000 from Paris VI University, France. In 2003, he received the Ph.D. degree in Physics at the Laboratoire Ondes & Acoustique in Paris for his work on the applications of the 1D shear elasticity probe and transient elastography. He is currently working toward a post-doc at the Laboratoire de Biorhéologie et d'Ultrasonographie Médicale in Montréal, Canada. His current research interests include blood rheology, vascular elastography, nonlinear shear waves, and soft tissues viscoelasticity.



**Thérèse Baldeweck** was born in Strasbourg, France, in 1969. She graduated from the engineering school Ecole Centrale de Lyon in 1992. She received the Ph.D. degree in Biomedical Engineering from the University of Paris VI for her work on ultrasonic attenuation measurements in highly attenuating media: application to skin characterization.

She is now a senior researcher in the advanced research laboratories of L'Oréal Group. Her research interests are ultrasonic

tissue characterization, new developments of high frequency ultrasound, and more generally new non-invasive methods for *in vivo* skin characterization.



**Mickaël Tanter** was born in December 1970 in Paimpol, France. He received the engineer degree in Electronics of SUPELEC in 1994. In 1999, he received the Ph.D. degree in physics (Acoustics) from the University of Paris VII for his work on the application of time reversal to ultrasonic brain hyperthermia. He is now a researcher in the National French Center of Science (C.N.R.S.) and in 2000 joined the laboratory Ondes et Acoustique at the Ecole Supérieure de Physique et de Chimie Industrielle de la ville de Paris (ESPCI). His current

research interests include wave focusing techniques in heterogeneous media, medical ultrasonic imaging, ultrasonic brain imaging, shear wave propagation in soft tissues for cancer detection, ultrasonic therapy, nonlinear acoustics, active noise control.



**Stefan Catheline** was born in 1970 in Ghardaia, Algeria. He received the DEA degree in acoustic physics in 1994 from Paris VI University, France. In 1998, he received his Ph.D. degree in physics from Paris VII (Denis Diderot) for his work on transient elastography. After a post doc at Scripps Institution of Oceanography, Marine Physical Laboratory, he became an assistant professor at Paris VII University in 1999 and joined the Laboratory Ondes et Acoustique at the Ecole Supérieure de Physique et de Chimie Industrielle de la

ville de Paris (ESPCI). His current research activities include shear waves in soft tissues and dynamic focusing using time reversal process in wave guides.



**Mathias Fink** received the diplôme de Doctorat de 3<sup>ème</sup> cycle in solid state physics in 1970 and the Doctorat ès-Sciences degree in acoustics in 1978 from the University of Paris VII, Paris, France.

From 1981 to 1984, he was a professor of acoustics at Strasbourg University, Strasbourg, France. Since 1984, he has been a professor of physics at the University of Paris VII (Denis Diderot), Paris, France. In 1990, he founded the Laboratoire Ondes et Acoustique at the Ecole Supérieure de Physique et

de Chimie Industrielles de la Ville de Paris (ESPCI). In 2002, he was elected to the French Academy of Technology. In 2003, he was elected to the French Academy of Science.

His current research interests include medical ultrasonic imaging, ultrasonic therapy, nondestructive testing, underwater acoustics, ac-

tive control of sound and vibration, analogies between optics and acoustics, wave coherence in multiple scattering media, and time reversal in physics. He has developed different techniques in speckle reduction, wave focusing in inhomogeneous media, and ultrasonic laser generation. He holds 28 patents, and he has published more than 300 articles.



**Laurent Sandrin** was born in Massy, France, on March 21, 1973. He received an Ing. degree from the Ecole Supérieure de Physique et de Chimie Industrielles de la Ville de Paris (ESPCI) with a specialization in physics in 1996. In 1994, he worked at the Sony Research Center in Yokohama (Japan) on large band-gap semiconductors for blue laser diodes. In 1996, he joined the Génie Physique Department of the Ecole Polytechnique de Montréal, Canada, to study the adhesion between metals (Al, Cu) and polymer

films (PE, PET). In 2000, he received the Ph.D. at the Laboratoire Ondes & Acoustique in Paris, where he has worked on elastography as well as ultrafast imaging under the supervision of Mathias Fink. Since then, he has been working for Echosens, which specializes in developing medical equipment using ultrasound for elastographic measurements.



**Céline Cornillon** was born in France in 1972. She graduated from the Créteil Technology Institute, France, in 1992.

She is currently a senior technician in the advanced research laboratories of L'Oréal Group. Her research interests concern the validation process of new non-invasive methods for *in vivo* skin characterization, and more particularly of high-frequency ultrasound imaging.



**Bernard Querleux** was born in France, in 1957. He received the Diploma degree in Electronic Engineering and the Ph.D. degree in Electronic Engineering and Signal Processing from the University of Grenoble, France, in 1983 and 1987, respectively. He got his Habilitation in Physics from Paris-Sud University in 1995.

He is currently a senior researcher in the advanced research laboratories of L'Oréal Group. His research interests include on one part the development of new non-invasive methods for skin imaging, and on another part the development of functional brain imaging methods for the objective assessment of sensory perception.